Lateral and vertical characteristics of floodplain aggradation cycles in the lower Eocene Willwood Formation, Bighorn Basin, Wyoming, USA

Wang, Youwei; Baars, Timothy F.; Storms, Joep E.A.; Martinius, Allard W.; Gingerich, Philip D.; Chmielewska, Magda; Buckley, Simon J.; Abels, Hemmo A.

DOI
10.1130/B36908.1

Publication date
2024

Document Version
Final published version

Published in
Bulletin of the Geological Society of America

THE GEOLOGICAL SOCIETY OF AMERICA®

Lateral and vertical characteristics of floodplain aggradation cycles in the lower Eocene Willwood Formation, Bighorn Basin, Wyoming, USA

Youwei Wang[1,2,†], Timothy F. Baars[1], Joep E.A. Storms[1], Allard W. Martinius[1,3], Philip D. Gingerich[4], Magda Chmielewska[5], Simon J. Buckley[6], and Hemmo A. Abels[1]

[1]*Department of Geosciences and Engineering, Delft University of Technology, Stevinweg 1, 2628 CN Delft, The Netherlands*
[2]*Department of Environmental Sciences, University of Virginia, Charlottesville, Virginia 22903, USA*
[3]*Equinor ASA, Arkitekt Ebbellsvei 10, N-7053 Trondheim, Norway*
[4]*Museum of Paleontology, University of Michigan, Ann Arbor, Michigan 48109-1079, USA*
[5]*Department of Geology and Petroleum Geology, University of Aberdeen, Aberdeen AB24 3UE, UK*
[6]*Norwegian Research Centre (NORCE), P.O. Box 22, N-5838 Bergen, Norway*

ABSTRACT

Sedimentation on river floodplains is a complex process that involves overbank flooding, crevasse splaying, and river avulsion. The resulting floodplain stratigraphy often exhibits floodplain aggradation cycles with alternating fine-grained overbank flooding deposits that underwent significant petrogenesis, and coarser-grained, avulsion-belt deposits largely devoid of pedogenic impact. These cycles are linked to lateral migration and avulsion of channels driven by internal dynamics, external factors, or a combination of both. To better understand the spatial and vertical variability of such floodplain aggradation cycles, we map these in three dimensions using a photogrammetric model of the lower Eocene Willwood Formation in the northern Bighorn Basin, Wyoming, USA. This allows identifying 44 floodplain aggradation cycles in ~300 m of strata with an average thickness of 6.8 m and a standard deviation of 2.0 m. All the cycles are traceable over the entire model, pointing to their spatial consistency over the 10 km^2 study area. At the same time, rapid lateral thickness changes of the floodplain aggradation cycles occur with changes up to 4 m over a lateral distance of 400 m. Variogram analyses of both field and numerical-model results reveal stronger consistency of floodplain aggradation cycle thicknesses along the paleoflow direction compared to perpendicular to paleoflow. Strong compensational stacking occurs at the vertical scale of 2–3 floodplain aggradation cycles (14–20 m), while full compensational stacking occurs at larger scales of more than six floodplain aggradation cycles (>41 m). The lateral and vertical thickness variability of the floodplain aggradation cycles, as well as their compensational stacking behavior, are interpreted to be dominantly driven by autogenic processes such as crevasse splaying and avulsing that preferentially fill topographic lows. External climate forcing may have interacted with these autogenic processes, producing the laterally persistent and vertically repetitive floodplain aggradation cycles. The spatial variability of floodplain aggradation cycles demonstrated in this study highlights again the need for three-dimensional data collection in alluvial floodplain settings rather than depending on one-dimensional records.

INTRODUCTION

Alluvial stratigraphy is primarily shaped by channel migration and avulsion as well as local and regional accommodation (Allen, 1978, 2008; Ashworth et al., 2004; Hajek and Wolinsky, 2012). Analysis of alluvial stratigraphy is commonly performed by examining the distribution and configuration of channel sandstone bodies and accompanying floodplain sediments (Allen, 1978; Bridge and Leeder, 1979). River avulsion is an important process in channelized depositional systems, occurring when a riverbed is sufficiently superelevated above the surrounding floodplain, and a triggering event (e.g., flood, log, or ice jam) permanently diverts flow out of the original channel (Jerolmack and Mohrig, 2007; Jones and Schumm, 1999; Karssenberg and Bridge, 2008; Mohrig et al., 2000; Slingerland and Smith, 2004). Avulsions can be distinguished as diverting channels at a local or regional scale (Slingerland and Smith, 2004). Both local and regional avulsions can be dominated by autogenic processes, such as lateral channel migration and crevasse splaying, while they are also subject to the influence of external forcings including climate, tectonics, and base-level changes (Kraus and Aslan, 1993; Slingerland and Smith, 2004; Atchley et al., 2004; Cleveland et al., 2007; Simpson and Castelltort, 2012; Abels et al., 2013; Burgess, 2016a, 2016b; Chadwick et al., 2022).

Well-documented floodplain successions from various basins typically demonstrate alternating units of fine-grained mature paleosols and pedogenically undisturbed heterolithic packages, including the Devonian of East Greenland (Olsen, 1994), the Carboniferous of the Upper Silesian Basin (Opluštil et al., 2022), the Middle Permian of the Karoo Basin in South Africa (Lanci et al., 2022), the Triassic of New Mexico, USA (Cleveland et al., 2007), the Cretaceous–Paleogene of West Texas, USA (Atchley et al., 2004), the Eocene of northern Wyoming, USA (Gingerich, 1969; Kraus and Aslan, 1993; Clyde and Christensen, 2003; Abels et al., 2013), among many others. These successions are interpreted to represent alternating overbank deposition that facilitate pedogenesis as well as crevasse-splaying and avulsion-belts resulting in heterolithic packages (Kraus, 1987; Kraus and Aslan, 1993; Atchley et al., 2004; Cleveland et al., 2007; Abels et al., 2013).

Alternating floodplain sedimentary units of fine clastics on which mature paleosols developed and pedogenically undisturbed, coarser-grained heterolithic packages on the floodplains of the Paleocene Fort Union and lower Eocene Willwood formations in the Bighorn Basin of Wyoming (Fig. 1) have been

Youwei Wang https://orcid.org/0000-0003-1583-8415
†youweiwang2021@outlook.com

GSA Bulletin; May/June 2024; v. 136; no. 5/6; p. 2568–2581; https://doi.org/10.1130/B36908.1.
Published online 18 October 2023

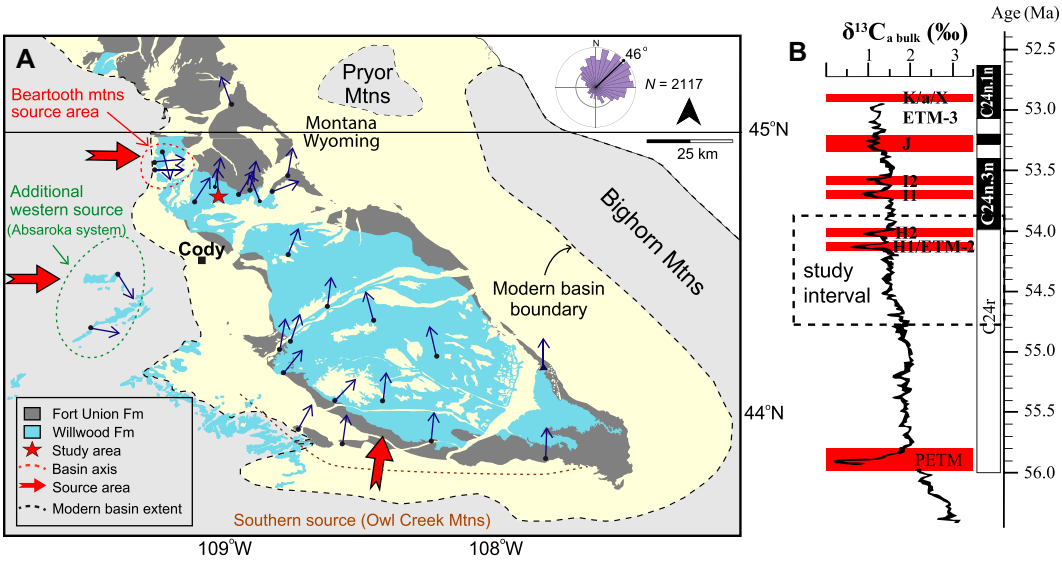

Figure 1. The study area and stratigraphy. (A) Geographic location of the study area, McCullough Peaks, and the provenances of the Bighorn Basin, Wyoming, USA (after Owen et al., 2017), with blue arrows indicating paleoflow directions. (B) The study succession with estimated position (dashed lines) in the stratigraphy based on $\delta^{13}C_{a\ bulk}$ data adjusted from Zachos et al. (2010) to the Gradstein et al. (2012) global time scale (Vandenberghe et al., 2012) by Birgenheier et al. (2020), with red-filled rectangles indicating hyperthermal events. ETM—Eocene Thermal Maximum; Fm—Formation; Mtns—Mountains; N—number of samples; PETM—Paleocene–Eocene Thermal Maximum.

described in detail (Kraus and Aslan, 1993; Abels et al., 2013). The floodplain aggradation cycles have been attributed to dominant autogenic processes, such as river migration and avulsion (Kraus and Aslan, 1993; Clyde and Christensen, 2003) as well as to allogenic factors that impact these autogenic processes, including climate, tectonics, and base level (Kraus and Aslan, 1993; Atchley et al., 2004; Cleveland et al., 2007). These alternating units show a consistent vertical repetition in various successions with an estimated periodicity of 20 k.y., which led to relating them to climatic variations driven by the orbital precession cycle (Kraus and Aslan, 1993; Abdul Aziz et al., 2008; Abels et al., 2013, 2016; van der Meulen et al., 2020). Based on detailed sedimentological description and statistical analysis, Abels et al. (2013) introduced a floodplain depositional model to interpret the observed patterns, which consists of two phases: an "overbank phase" characterized by the development of mature paleosols during intervals of relative channel stability, followed by an "avulsion phase" where regional avulsion and crevasse splaying resulted in coarser-grained heterolithic deposits (Figs. 2A and 2B) and relative channel instability. In this study, we use the term "floodplain aggradation cycle" to denote these two alternating units formed during the *overbank* and *avulsion* phases, respectively (Figs. 2A and 2B). Wang et al. (2021) elaborated on this model through a numerical stratigraphic forward modeling study that replicated broadly similar depositional patterns to those observed in the Bighorn Basin. Their study relates the phases of channel avulsion and rapid deposition to increased sediment load and the phases of channel stability and low deposition to reduced sediment load (Fig. 2C).

Previous studies have examined the characteristics and age of these floodplain aggradation cycles in one-dimensional (1-D) stratigraphic sections (Abdul Aziz et al., 2008; Abels et al., 2013), while more recent studies have included age control and correlation of coeval floodplain aggradation cycles across parallel sections at a kilometer scale (Abels et al., 2016; Westerhold et al., 2018; van der Meulen et al., 2020). However, these studies have not yet investigated the lateral and vertical variability of these floodplain aggradation cycles in continuous outcrops. While regional climate conditions are expected to exert consistent or comparable effects on regional stratigraphy, local processes such as channel migration, splaying, and avulsion could create strong stratigraphic signatures as well.

To address these knowledge gaps, we present a study tracing the floodplain aggradation cycles in the Willwood Formation of the McCullough Peaks area in the northern Bighorn Basin. Using an unmanned aerial vehicle (UAV)-based photogrammetric model, we demonstrate the traceability of floodplain aggradation cycles over a large area, quantify the lateral and vertical thickness variability of these floodplain aggradation cycles, and analyze their compensational stacking behavior, showcasing the mixed influences of autogenic processes and allogenic factors.

GEOLOGICAL SETTING

The Bighorn Basin during the Paleocene to early Eocene was bordered by the Beartooth Mountains to the west, the Washakie Range to the southwest, the Bighorn Mountains to the east, and the Pryor Mountains to the northeast (Fig. 1; Lillegraven and Ostresh, 1988). The paleo-fluvial system of the Willwood Formation drained toward the north and northeast, with provenances from mountainous areas expressed before or during the early Eocene (Neasham and Vondra, 1972; Kraus and Middleton, 1987; Owen et al., 2019; Wang et al., 2022).

Floral and faunal fossils have been extensively studied in the basin to understand the paleoenvironments and paleoclimates, and these records are integrated with other stratigraphic controls such as magnetostratigraphy, chemostratigraphy, and tephrastratigraphy (Clyde et al., 1994; Gingerich, 2010). These controls suggest that basin subsidence during the Paleocene and Eocene was at a quasi-constant rate of 329 m/m.y. (Foreman, 2014; Abels et al., 2013, 2016).

The study area in the McCullough Peaks, located in the northwest of the Bighorn Basin (Fig. 1), includes deposits formed during the Eocene Thermal Maximum 2 (ETM2) and subsequent H2 events (Abels et al., 2016). Previous work by Abels et al. (2012, 2013, 2016) provides a foundation for this study, as they conducted detailed field descriptions and analyses from several trenched sections down to fresher rocks. Particularly, our work is built upon

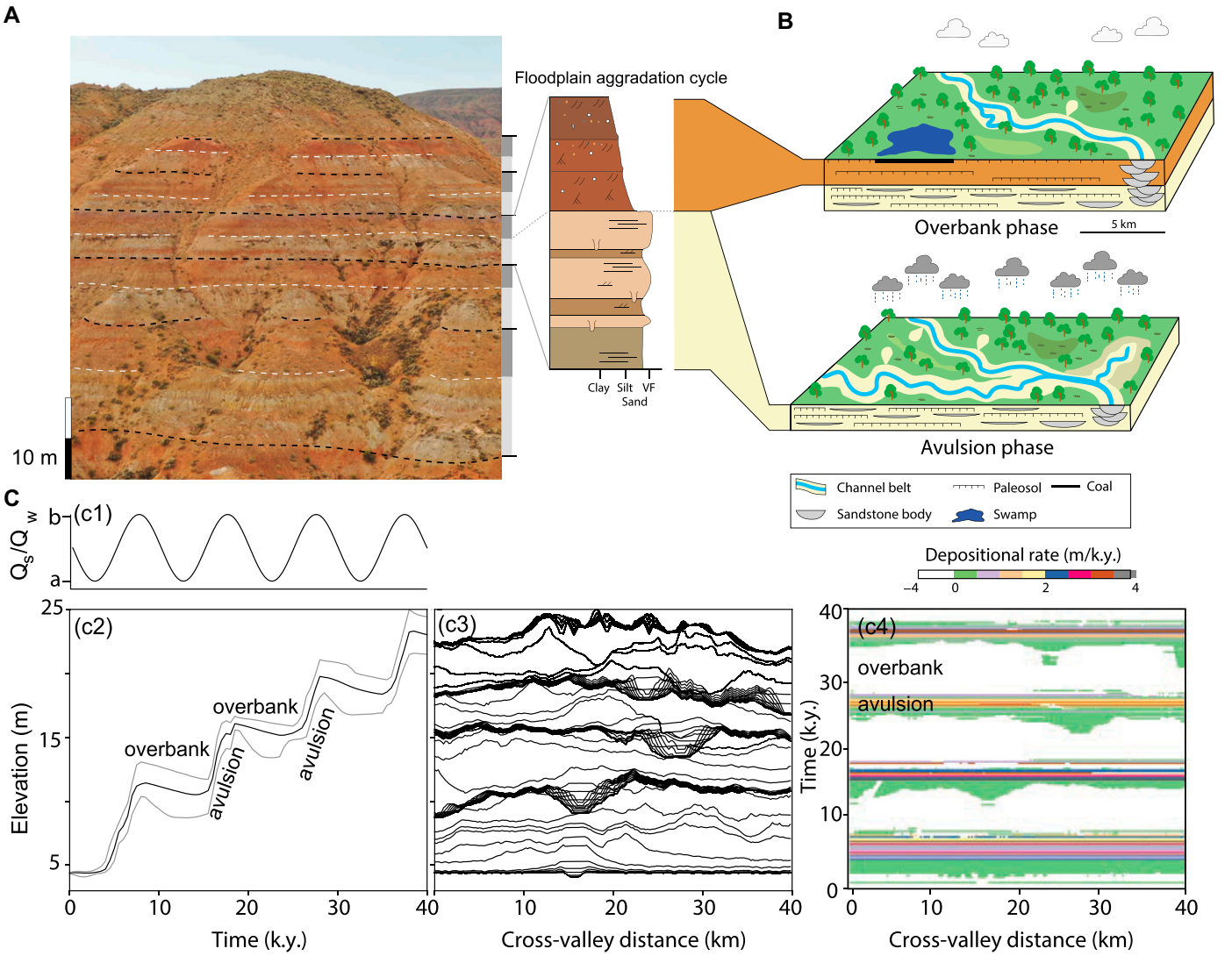

Figure 2. Definition and depositional models of floodplain aggradation cycles as well as their numerical analogs. (A) A field photograph accompanied by sedimentological descriptions displaying alternating units of mature paleosols (as indicated by the dark gray column adjacent to the photo) and undisturbed heterolithic deposits (represented by the light gray column). These elements clarify the definition of floodplain aggradation cycles in our study. For detailed sedimentologic work, please refer to Abels et al. (2012, 2013, 2016) as it is not presented here in detail. (B) Depositional models for the regular alternation of mature paleosols and undisturbed heterolithic deposits observed in the Bighorn Basin, Wyoming, USA. These are interpreted to form during two distinct phases: the overbank phase, characterized by relatively stable channel positions and mature soils; and the avulsion phase, characterized by unstable channel positions and undeveloped heterolithic deposits. This subfigure is adapted from Abels et al. (2013). (C) Numerical modeling results that illustrate alternating phases of fast deposition (analogous to the avulsion phase) and low-to-non-deposition (resembling the overbank phase). This is adapted from figure 8 in Wang et al. (2021). The model employs cyclic sediment supply and water discharge (panel c1), resulting in phases of channel stability (as shown by the horizontal part in panel c2, condensed timelines in panel c3, and high depositional rate in panel c4) and channel instability (as indicated by the climbing part in panel c1, separated timelines in panel c2, and overall non-deposition and in-channel deposition in panel c3). These phases are evident in a cross section from the middle part of the basin (for additional details, see Scenario A40 of figure 8 in Wang et al., 2021). The third cycle of this scenario, as denoted in panel c3, is further analyzed in Figure 11. VF—very fine.

the depositional model in Abels et al. (2013) where an "overbank phase" is characterized by the development of mature paleosols during intervals of channel stability, followed by an "avulsion phase" where regional avulsion and crevasse splaying result in coarser-grained heterolithic deposits (Fig. 2). Deposits of these two phases form the subject of this study—floodplain aggradation cycles. Wang et al. (2022) measured paleoflow directions from dune-scale cross-stratification, mainly planar and trough cross-stratification, in channelized sandstone bodies, which are used as the regional paleoflow direction in this study.

METHODOLOGY

UAV-Based Photogrammetry

Photographs were taken automatically every three seconds by a 20-megapixel camera mounted on a multirotor DJI Phantom 4 Pro

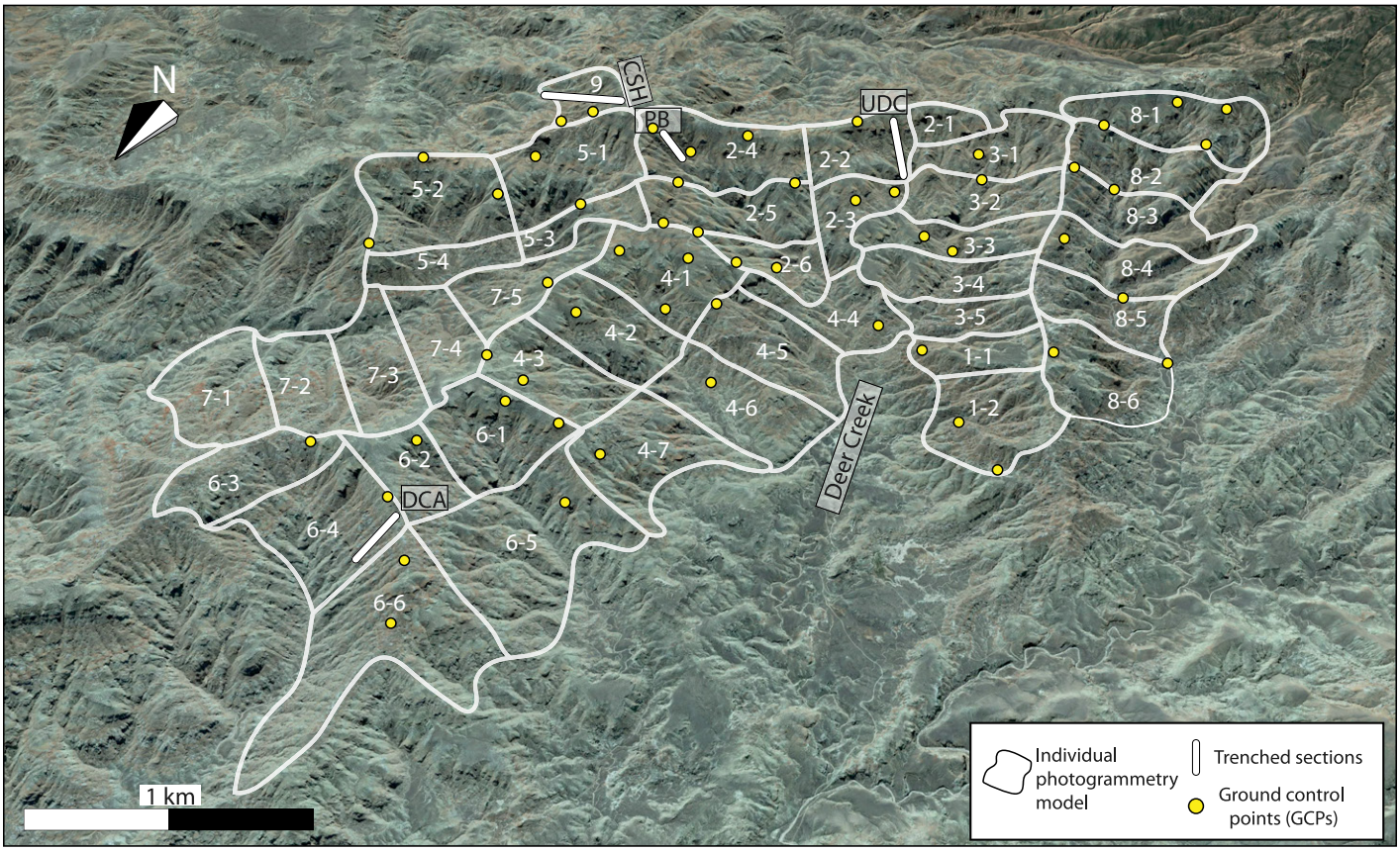

Figure 3. Bird's-eye view from Google Earth illustrating the location of 42 individual photogrammetric 3-D models in the McCullough Peaks area (Wyoming, USA). The Deer Creek Amphitheater section (DCA) (Abels et al., 2013), Purple Butte section (PB), Upper Deer Creek section (UDC) (Abels et al., 2012), and Creek Star Hill section (CSH) (Abels et al., 2016) are abbreviated.

UAV. The UAV was manually flown parallel to the outcrop surface at a speed of 5–10 m/s to ensure a 60% horizontal overlap between successive photos. A total of 21,144 photos were taken on 34 flights (Fig. 3), covering an area of ~10 km^2. The studied stratigraphic succession, dipping at ~2° toward the south, is roughly 300 m thick. To ensure accuracy, 57 ground control points (GCPs) were placed (Fig. 3) and surveyed using an Emlid Reach global navigation satellite system (GNSS) receiver, which was calibrated using the post-processed kinematic positioning technique. Raw GNSS measurements recorded by both the rover and base stations were processed using the open-source GNSS post-processing package RTKLIB, which allowed for the determination of the GCP positions with centimeter accuracy relative to the local base station.

To build the 3-D digital models, Agisoft PhotoScan (Version 1.4.3, July 2018; current Metashape) was utilized, which employed the structure-from-motion multi-view-stereo (SfM-MVS) photogrammetric method. A triangulated digital surface mesh was created, and the photos were draped onto the surface as the texture. To manage the large image set, the photogrammetric images were divided into 42 model sections, and a tiled model was generated for each section. The entire 3-D outcrop model was imported into LIME (version 2.2.2; Buckley et al., 2019) for visualization and interpretation.

Identification of Boundaries between Floodplain Aggradation Cycles

When tracing floodplain aggradation cycle boundaries, we found that the transition from fine siliciclastic with mature paleosols (usually red to purple in color) to sandier deposits with immature paleosols (usually pale brown, yellowish, or orange) is the most reliable indicator of boundary placement throughout the photogrammetric model. This differs from the approach taken by Abels et al. (2013), who typically located boundaries at the top of the strongest soil development index (SDI) values, often corresponding to the reddest soil on freshly exposed rock surfaces. However, in our models, weathering has made it difficult to identify the strongest SDI values, so we opted for a more consistent and reproducible approach across all floodplain aggradation cycles and among multiple interpreters (including three co-authors of this manuscript): tracing the red-to-yellow transitions that are most clear and leave less room for doubt. Our identified boundaries are always higher than, if not the same as, the boundaries of Abels et al. (2013) based on the SDI that is a function of horizon differentiation, soil thickness, and rubification. This approach helps to reduce interpretive bias and ensure greater applicability and consistency in our floodplain aggradation cycle boundary identification and interpretations.

Variogram Analysis

The variogram is a mathematical function that quantifies the dissimilarity between pairs of data points as a function of the separation distance or lag distance (h) (Pyrcz and Deutsch, 2003). Typically, the variogram values increase with lag distances, indicating increasing dissimilarity between the data points. A variogram can be calculated as follows (Pyrcz and Deutsch, 2003):

$$\gamma(h)=\frac{1}{2N(h)}\sum_{\alpha=1}^{N(h)}\left(z(u_\alpha)-z(u_\alpha+h)\right)^2, \quad (1)$$

where $\gamma(h)$ is a measure of dissimilarity between two data points over lag distance h, and the dissimilarity here refers to the difference of floodplain aggradation cycle thickness in this study; $N(h)$ is the number of data point pairs; u_α is a data point at location α in 2-D space; $u_\alpha + h$ is a data point separated from u_α by the distance h; $z(u_\alpha)$ is the numerical value at the data point u_α; and $z(u_\alpha + h)$ is the numerical value at the location $u_\alpha + h$.

To investigate the depositional patterns of floodplain aggradation cycles, we measured their thicknesses on outcrop surfaces in the model every 20 m when possible (Fig. S1A[1]). The variogram, from a predictive standpoint, offers insights into the isotropic or anisotropic nature of these thickness patterns. An isotropic pattern would be indicated by a variogram displaying monotonically increasing trends (Pyrcz and Deutsch, 2003). In contrast, anisotropic thickness patterns would manifest as non-monotonically increasing trends in the variogram (Pyrcz and Deutsch, 2003). Given the significant influence of channel belts in fluvial landscapes and stratigraphy, we anticipate anisotropic thickness patterns for floodplain aggradation cycles. These channel belts are expected to play a considerable role in shaping the thickness of such cycles.

In order to detect the possibly present anisotropic thickness patterns, we analyzed the measured floodplain aggradation cycle thicknesses using Python codes developed by Pyrcz (2020) to first derive the 2-D variogram map. Then, we calculated variograms in six directions with equal azimuth zones of 30°, 60°, 90°, 120°, 150°, and 180°, considering the observed statistical anisotropy. We set the lag distance to 100 m and the lag tolerance to 50 m. We used a search strategy with a wide azimuth tolerance of 30° and a large bandwidth of 2 km to reduce the nugget effect near the origin (Zhang et al., 2005). Identifying a range when the sill ($\gamma(h) = 1$) is reached in the directional variogram (Figs. S1B and S1C) indicates spatial continuity of floodplain aggradation cycle thickness, where thickness at one locality is stochastically related to that at another locality.

To help understand the relationship between variogram features and sedimentary processes, we also analyzed a numerical model of stratigraphy developed by Wang et al. (2021) for the third cycle in their Scenario A40 (Fig. 2C3). In this scenario, cyclic changes in water discharge and sediment supply with a wavelength of 10 k.y. and an amplitude of 40% produced four cycles that broadly matched the floodplain aggradation cycles in the Bighorn Basin. Our objective here is not to directly compare the absolute values of variograms given the challenges in direct field and model comparisons. Rather, our anticipation is to discern similar influences of channel belt orientation on the thickness patterns of these floodplain aggradation cycles, further demonstrating the relationship between these geological features and the corresponding processes.

Compensational Stacking Analysis

Compensational stacking refers to a phenomenon in depositional sediment transport systems, wherein preferential filling occurs in topographic lows (Straub et al., 2009; Straub and Pyles, 2012). To analyze compensational stacking, we use two metrics: the coefficient of variation (CV) and the compensational stacking index (σ_{ss}). In the present study, we adopt a unique perspective by considering floodplain aggradation cycles as the fundamental stratigraphic units. This represents a departure from past studies (e.g., Wang et al., 2011; Trampush et al., 2017), which primarily employed higher-resolution geological units. By designating floodplain aggradation cycles as the level of stratigraphic resolution, our objective is to determine the existence and scale of compensational stacking within alluvial stratigraphy. Furthermore, Wang et al. (2021) proposed that the influence of allogenic forcing could potentially impact the traditional estimation of the compensational time scale (T_c), which is conventionally approximated as the ratio of maximum relief to long-term sedimentation rate (Straub et al., 2020). Here we aim to juxtapose our findings with existing estimates to test the findings of Wang et al. (2021).

Coefficient of Variation

The coefficient of variation (CV) is defined as the ratio of the standard deviation over the mean of a data series (herein the measured series of floodplain aggradation cycle thickness), and thus, a smaller CV indicates less variability. To test compensational stacking, successive depositional units (floodplain aggradation cycles) are combined as assemblages, and the CV is calculated for each assemblage. For example, floodplain aggradation cycles 1 and 2 can be combined as an assemblage, and the thickness of the assemblage is rescaled by dividing it by the regional mean thickness. This rescaling allows for the comparison of thickness variation among different assemblages. An example of how CV is calculated for a stratigraphic interval with three floodplain aggradation cycles is provided in Supplemental Text S1 and Figure S2. In this study, we define an assemblage as strongly compensated when the CV value sharply drops, while we define it as fully compensated when the CV value stops decreasing and stabilizes.

Compensational Stacking Index

The standard deviation of sedimentation/subsidence (σ_{ss}) (Wang et al., 2011) can be used to characterize the compensational time scale:

$$\sigma_{ss}(T)=\left\{\int_0^L\left[\frac{r(T;x)}{\hat{r}(x)}-1\right]^2 dL\right\}^{1/2}, \quad (2)$$

where $r(T; x)$ is the average deposition rate at a horizontal coordinate of x during a time interval of T, L is the cross-basin length, and $\hat{r}(x)$ is the local long-term sedimentation rate.

Theoretically, σ_{ss} is expected to decrease as T increases, following a power-law trend (Equation 3, Straub et al., 2009; Wang et al., 2011):

$$\sigma_{ss} = a'T^{-\kappa}, \quad (3)$$

where a' is a coefficient, and κ is termed the compensation index.

By reorganizing Equation 3, we can get:

$$\log(\sigma_{ss}) = \log(a') - \kappa^*\log(T). \quad (4)$$

Therefore, the slope is $-\kappa$, and the intersection is log (a') for the relationship between log (T) and log (σ_{ss}).

Straub and Wang (2013) provide an intuitive illustration of the T_c, which can be used to differentiate between stratigraphy that is partially influenced by autogenic forcing and stratigraphy that is solely influenced by allogenic forcing (see fig. 2 in Straub and Wang, 2013). As shown in figure 3 in Wang et al. (2011), T_c is characterized by a value of $\kappa = 1$, indicating that the stratigraphic stacking is purely compensational beyond this time scale (Straub et al., 2009). A practical workflow to identify the T_c is presented in Supplemental Text S2.

[1]Supplemental Material. Supplemental Text S1: More detailed workflow about the coefficient of variation (CV) calculation. Supplemental Text S2: More detailed workflow about the calculation and application of compensational stacking index. Table S1: Geostatistical features of thicknesses of different floodplain aggradation cycles. Figure S1: Example data distribution and schematic illustration of variogram components. Figure S2: An example showing how CV is calculated. Please visit https://doi.org/10.1130/GSAB.S.24128637 to access the supplemental material, and contact editing@geosociety.org with any questions.

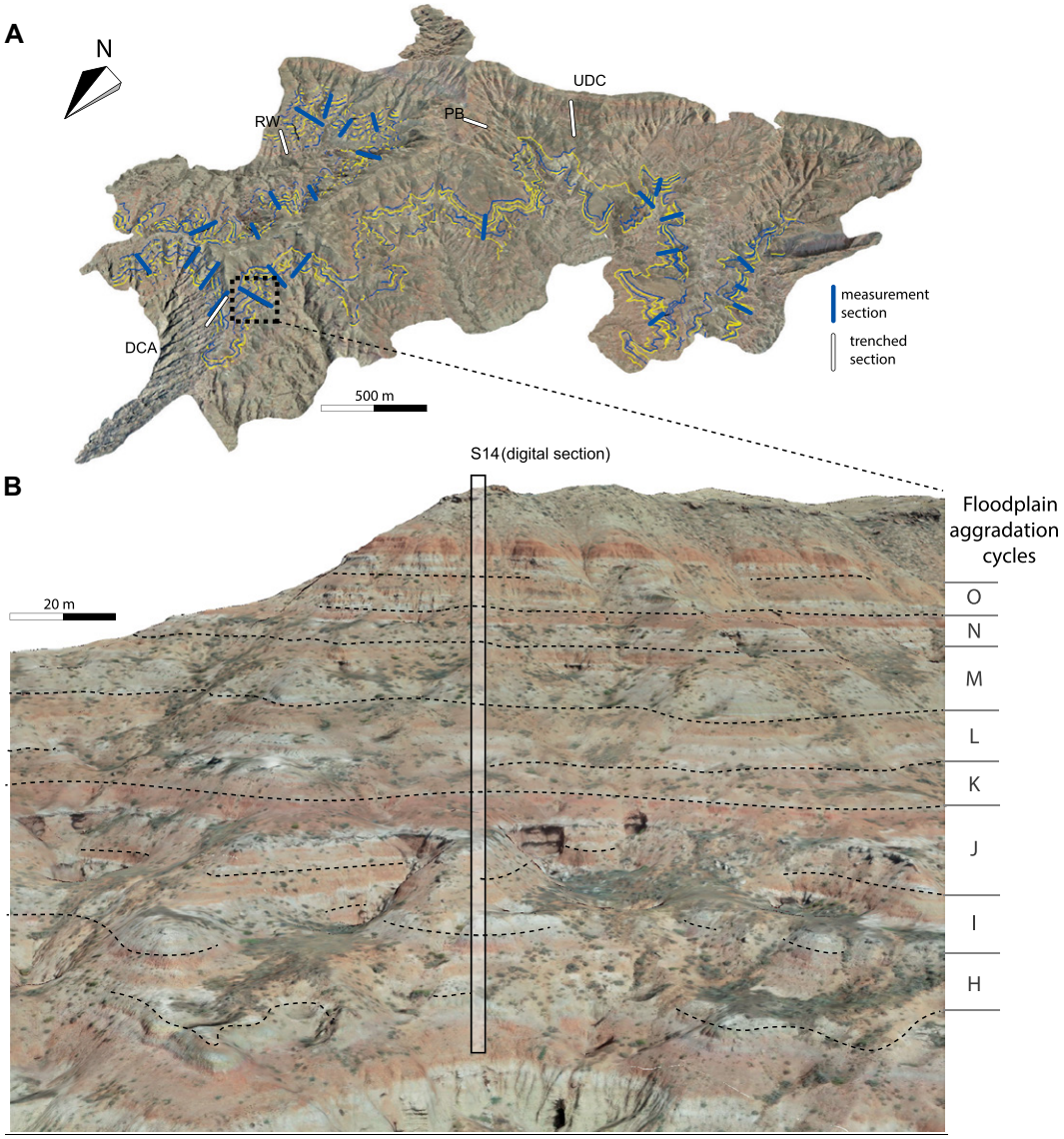

Figure 4. Floodplain aggradation cycles are traced using both photogrammetric models and individual unmanned aerial vehicle and camera photos. (A) The interpreted 3-D photogrammetric model in the McCullough Peaks area (Wyoming, USA) provides an overview, depicting traced boundaries for seven successive floodplain aggradation cycles. (B) Zoomed-in outcrop section in the 3-D model revealing how floodplain aggradation cycle boundaries (blue and yellow lines) are traced and how a digital section (S14) is selected from model data. CSH—Creek Star Hill; DCA—Deer Creek Amphitheater; PB—Purple Butte; UDC—Upper Deer Creek.

RESULTS

Tracing of Floodplain Aggradation Cycles

Our study has identified a total of 44 floodplain aggradation cycles within a ~300-m-thick succession (Fig. 4A). This succession begins seven floodplain aggradation cycles below the base of the Deer Creek Amphitheater section of Abels et al. (2013) and ends slightly above the top of the Upper Deer Creek section of Abels et al. (2012) and the Creek Star Hill section of Abels et al. (2016). The lower 10 floodplain aggradation cycles and upper 11 floodplain aggradation cycles have limited lateral extents within the photogrammetric model, while most of the other floodplain aggradation cycles can be traced over distances up to 4 km in the NE-SW direction and ~2.5 km in the SE-NW direction. A composite section that includes all the 44 floodplain aggradation cycles is constructed by combining data from available trenched sections (Deer Creek Amphitheater, Creek Star Hill, and Upper Deer Creek sections; Abels et al., 2012, 2016). To maintain consistency, we have extended the labeling system of Abels et al. (2013) and Abels et al. (2012) rather than introducing a new one (Fig. 5). Our floodplain aggradation cycles P1 to P3 correspond to ETM2, while floodplain aggradation cycles P5 to P8 correspond to H2 (Abels et al., 2012, 2016; Fig. 1).

Among the 44 floodplain aggradation cycles, seven successive floodplain aggradation cycles with the largest exposure area in our photogrammetry models were traced continuously in the lateral extent through the whole model (Fig. 4B) by following regionally persistent boundaries described in the Methodology section. The boundaries between the cycles in this study are on average 0.6 m higher than those defined by Abels et al. (2013) in their composite trenches (Fig. 6). Despite this difference, our boundaries are still effective at separating the overbank phase of the lower floodplain aggradation cycle from the avulsion phase of the upper floodplain aggradation cycle.

Local factors can complicate the lateral tracing of floodplain aggradation cycle boundaries. These factors include the presence of channel sandstone bodies, the splitting or merging of paleosol horizons, the occurrence of debris and vegetation covering outcrops, and areas of low resolution in the photogrammetric models. In some cases, we found that the most distinctive red/purple to yellow sediment color transitions occur at different stratigraphic levels laterally, with offsets of a few decimeters to 1–2 m. In these cases, we tried to maintain consistency by placing the overbank to avulsion phase transition at the stronger of the two transitions and

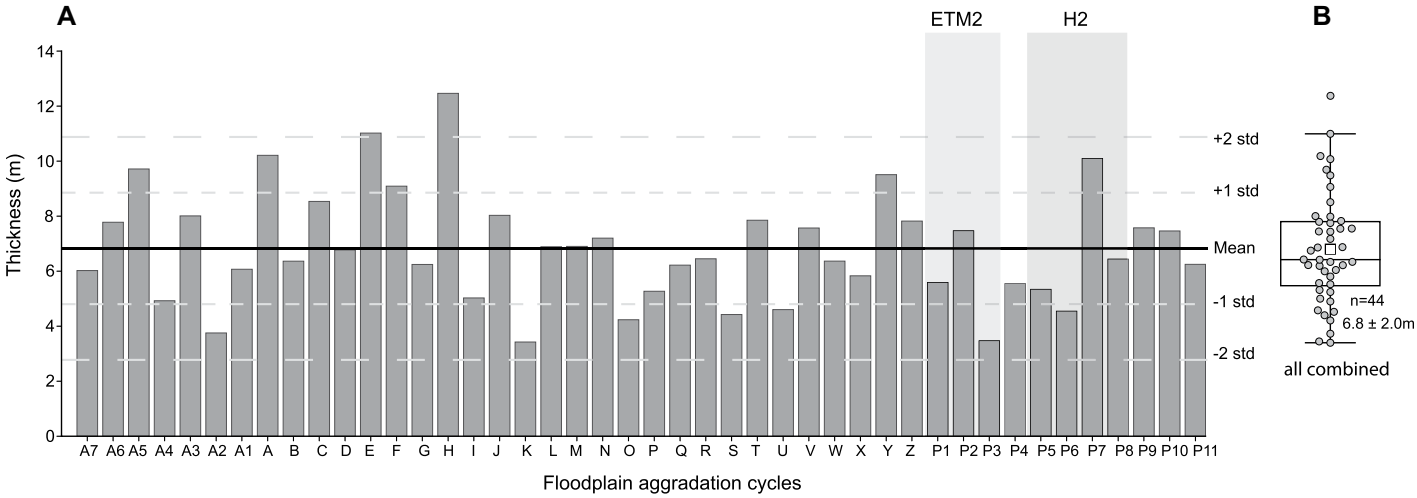

Figure 5. Thicknesses of 44 floodplain aggradation cycles in the composite stratigraphy of the McCullough Peaks area (Wyoming, USA). (A) The bar diagram depicts the labeling system and the variability in floodplain aggradation cycle thickness. (B) The boxplot shows the mean (6.8 m), standard deviation (2.0 m), and coefficient of variation (standard deviation/mean; 29%) of these 44 floodplain aggradation cycles' thicknesses. The box boundaries represent lower and upper quartiles, lines extending from boxes indicate the 1st to 2nd and 3rd to 4th quartile ranges, lines and squares within boxes indicate median and mean values, and points outside boxes represent outliers. The meaning and stratigraphic positions of ETM2 and H2 are illustrated in Figure 1B. n—number of samples; std—standard deviation.

tracing it laterally across the model. Nevertheless, this kind of uncertainty only occurs at a few locations where crevasse-splay deposits are dominant, and strong, exclusive traceability returns after crossing these crevasse-splay deposits.

Lateral Thickness Variability of Individual Floodplain Aggradation Cycles

To analyze the thickness variability and spatial correlation of individual cycles, seven extensively exposed floodplain aggradation cycles in the middle of the studied stratigraphy were traced in detail over the whole photogrammetric model. These floodplain aggradation cycles are labeled H to N. The regionally averaged thicknesses of individual floodplain aggradation cycles vary between 3.7 m (cycle K) and 9.7 m (cycle L) with a CV range of 17% to 28%. The average thickness of all seven floodplain aggradation cycles is 7.3 m with a standard deviation of 2.6 m (Fig. 7).

A total of 22 digital sections, such as section 14 (S14) shown in Figure 3B, were created in the photogrammetric model, with floodplain aggradation cycle N as horizontal reference level (Fig. 8). These sections reveal that the thicknesses of these floodplain aggradation cycles vary rapidly in the lateral direction, with a maximum of 4 m over a lateral distance of 400 m.

To investigate the spatial correlation of floodplain aggradation cycle thicknesses, variograms were calculated for each of the seven floodplain aggradation cycles studied in detail. The correlatable distance is on average 1.3 km in the long-range direction and 0.6 km in the short-range direction (Fig. 9A; Table S1). The aspect ratio (i.e., long range/short range) of the variogram ellipse ranges from 1.4 to 5.3, with an average of 2.2 (Table S1). The long-range azimuth ranges between N 310° and N 080°, averaging N 001° (Fig. 9B; Table S1). This is consistent with the average paleoflow direction measured in the dune-scale cross-beddings in the field (N 004° ± 24°; Fig. 9C; after Wang et al., 2022). Different from the classic 1-D variograms that exhibit monotonically increasing patterns, we observe non-monotonic patterns in variograms along certain azimuth directions (as annotated along azimuth 125°, e.g., in Fig. 10).

A similar analysis was employed on the numerical model data from Wang et al. (2021) to investigate the thickness variability and spatial correlation of the stratigraphic cycles (Fig. 11). The thickness map of the third cycle in the center of the basin was used to avoid the influence of boundary effects exerted by sediment supply at the basin inlet and base-level rise near the basin outlet (Fig. 11C). The variogram analysis of the modeled data reveals a long range of 22 km in the paleoflow direction and a short range of 6 km perpendicular to paleoflow direction (Fig. 11D). Similar to the field data, non-monotonic patterns are observed in variograms of numerical model data (e.g., azimuth N 030°, Fig. 11D), which may relate to the presence of major channel belts.

Vertical Thickness Variability of Floodplain Aggradation Cycles

The thickness of floodplain aggradation cycles varies locally and can display significant vertical variability. Thicker floodplain aggradation cycles are often resting on the top of thinner ones, and vice versa. For example, in S18 (see Fig. 8), a thick floodplain aggradation cycle (L) is overlain by a thinner one (M). Similarly, the 1-D composite section consisting of 44 floodplain aggradation cycles (Fig. 5) displays significant vertical variability in floodplain aggradation cycle thicknesses, with an average thickness of 6.8 m and a standard deviation of 2.0 m.

Compensational stacking, during which successive floodplain aggradation cycles offset the thickness variations of one another, can reduce the thickness variability of a stratigraphic assemblage containing several floodplain aggradation cycles. To investigate this compensational stacking, the CVs of seven floodplain aggradation cycles in the 22 digital sections (Fig. 8) are calculated (Fig. 12). Assemblages of two successive floodplain aggradation cycles have a much smaller CV (14%) than those with one floodplain aggradation cycle (23%). Assemblages containing six or more successive floodplain aggradation cycles have a stabilized CV of 6%, indicating full compensation. Calculation of the compensational stacking index shows the scale-dependent decay of σ_{ss} (Fig. 12), indicating stronger compensation over a longer time (Straub et al., 2009; Wang et al., 2011; Straub and Wang, 2013). The

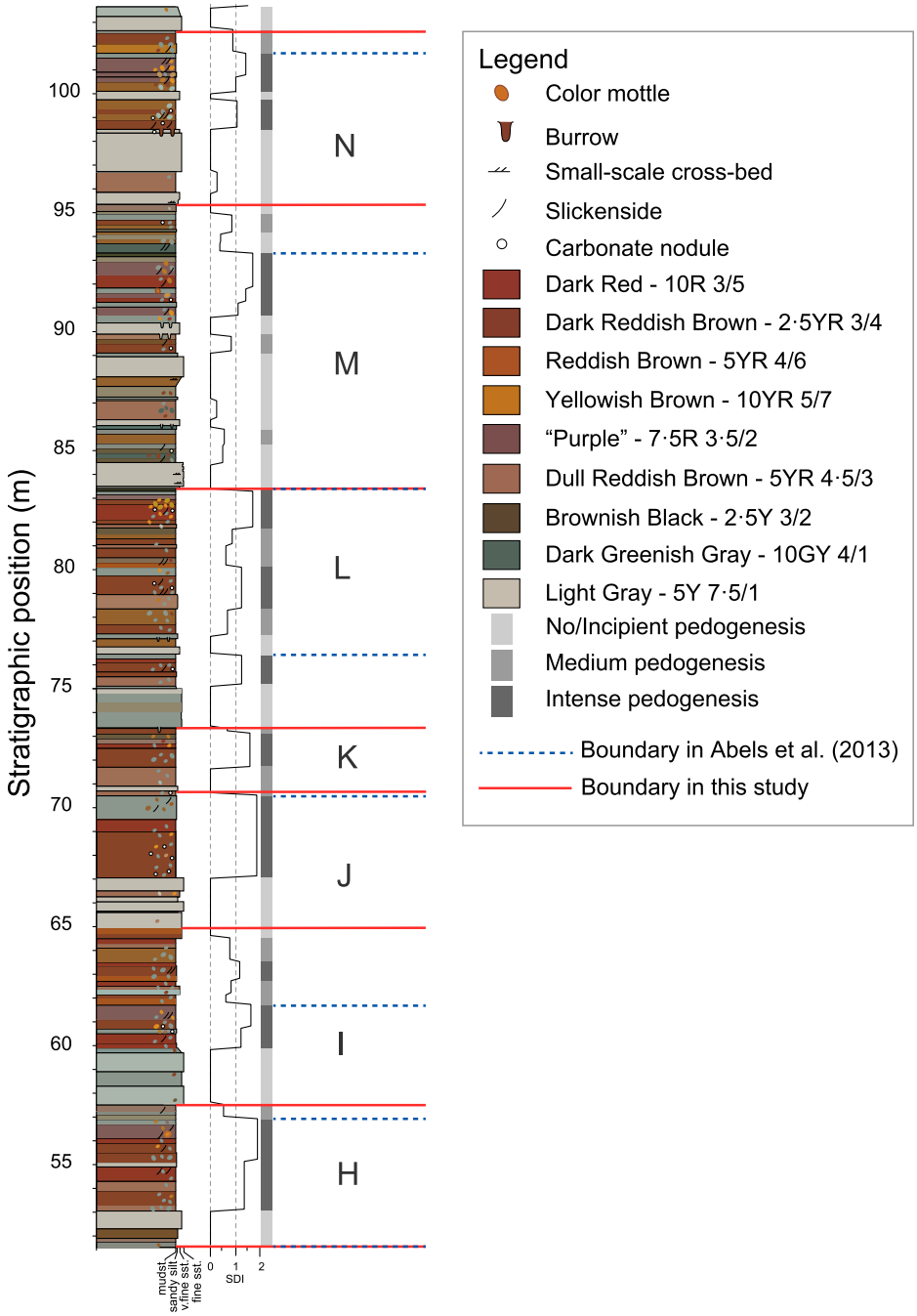

Figure 6. Comparison of floodplain aggradation cycle boundaries in this study (red line) and cycle boundaries by Abels et al. (2013) (blue dashed line) for floodplain aggradation cycles H–N in the McCullough Peaks area (Wyoming, USA). The curve of the Soil Development Index (SDI) is a function of paleosol B horizon thickness, horizon development intensity, and B-horizon rubification (Abels et al., 2013). mudst.—mudstone; v. fine sst.—very fine sandstone.

strength of compensation, as quantified by κ, has a lower magnitude of 0.53 within the determined T_c, which is ~12 floodplain aggradation cycles, indicating random to compensational filling (κ = 0.5–0.75) that is mostly driven by autogenic forcing (Straub and Wang, 2013). When the stratigraphic assemblage contains more than 12 floodplain aggradation cycles, κ approaches 1, indicating full compensation.

DISCUSSION

Meter-scale floodplain aggradation cycles are dominant features in many alluvial records (e.g., Kraus and Aslan, 1993; Abels et al., 2013; Atchley et al., 2013). They have been related to (1) phases of river stability and overbank deposition on which mature paleosols developed and (2) phases of regional-scale river avulsion causing deposition of the heterolithic, sandy avulsion belts on which immature soils developed (Kraus and Aslan, 1993; Abels et al., 2013; Noorbergen et al., 2018, 2020; Opluštil et al., 2022). In this study, we investigate the spatial character of these floodplain aggradation cycles in a 10 km^2 area of the northern Bighorn Basin, Wyoming, to quantify their lateral and vertical variability, the results of which will be discussed in the following sections.

Lateral Thickness Variability of Floodplain Aggradation Cycles

The Willwood Formation floodplain aggradation cycles display significant lateral thickness variation, as observed in quasi-continuous outcrops of the McCullough Peaks area. In some instances, the thickness of a single cycle can differ by up to four times between locations when comparing the maximum thickness with the minimum (Fig. 7). The tracing of floodplain aggradation cycles in photogrammetry models has an uncertainty of 1–2 m, but we do not regard this to significantly affect the overall mapping results.

Differential consolidation and compaction between different lithologies in the compacted stratigraphy may have played a significant role during and after deposition (Törnqvist et al., 2008). Sand-rich deposits are more resistant to consolidation and later compaction compared to clay-rich deposits. In our data, thicker-than-average floodplain aggradation cycles at local sections are often sand-rich. This could be due to high sedimentation rates of sand-rich depositional processes, but also due to lower compaction of these facies. However, it is difficult to determine the extent to which this variability is related to early consolidation or later compaction. We found that dynamic backstripping is needed, as simple linear backstripping resulted in unsatisfactory results. Dynamic backstripping (e.g., Célérier, 1988) requires substantial resources that were considered beyond the scope of the current study. Therefore, all of our findings are based on compacted stratigraphy.

The thickness variability is interpreted to relate to variable aggradation rates within different morphological elements of the Willwood Formation fluvial systems (Wang et al., 2022). Aggradation rates decrease away from channel belts; beyond channel aggradation, levee and crevasse splays host the highest aggradation

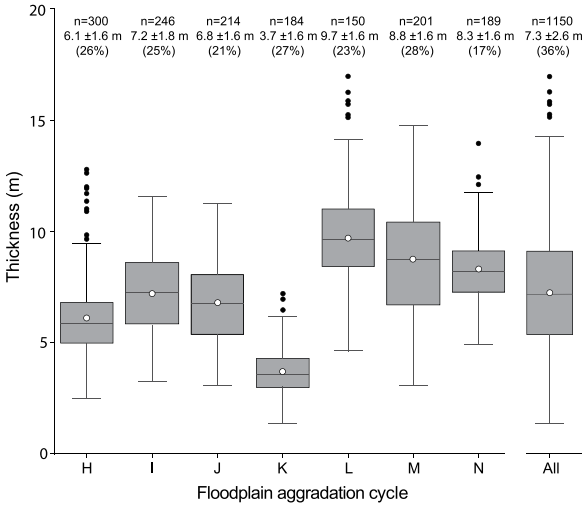

Figure 7. Box plots illustrating the thickness variability of floodplain aggradation cycles H–N in the McCullough Peaks area (Wyoming, USA). The very right box plot is based on 1150 measurements that are equally contributed by the seven floodplain aggradation cycles by randomly selecting 150 measurements from each floodplain aggradation cycle. Please refer to Figure 5 for an explanation of the components of the box plot. Note that the number combination of "a ± b (c)" above each box plot represents "regional average ± standard deviation (coefficient of variation)". n—number of samples.

rates, while purely fine-grained packages accumulate in distal floodplains (Mackey and Bridge, 1995; Kraus, 1999; Mohrig et al., 2000; Törnqvist and Bridge, 2002; Hajek and Straub, 2017). Rapid sedimentation in an area near the channel belt is accompanied by slow sedimentation on distal floodplains where only suspended load may arrive during peak floods. This variation in aggradation rates occurs within the same phase of the floodplain aggradation cycles, causing lateral thickness variability within the individual cycles.

Our observations indicate that the thicknesses of floodplain aggradation cycles are more consistent in the paleoflow direction, as demonstrated in both field and numerical-model data (Figs. 8–10). This consistency is likely related to the morphological segmentation of the Willwood Formation floodplains by channel belts that are dominantly oriented downstream. Previous studies have suggested that the Bighorn Basin was characterized by transverse river systems from the basin margins and axial river systems flowing north over the basin axis (Owen et al., 2019; Wang et al., 2022). The study area is located over the basin axis, and it seems unlikely that transverse and axial river systems interacted at this location. Although this scenario cannot be entirely excluded, the new data presented here indeed suggests a dominance of axial river systems draining toward the north and northeast in the study area.

The influence of paleoflow direction on floodplain sedimentation is seen in both numerical-model and field data. For a single fluvial

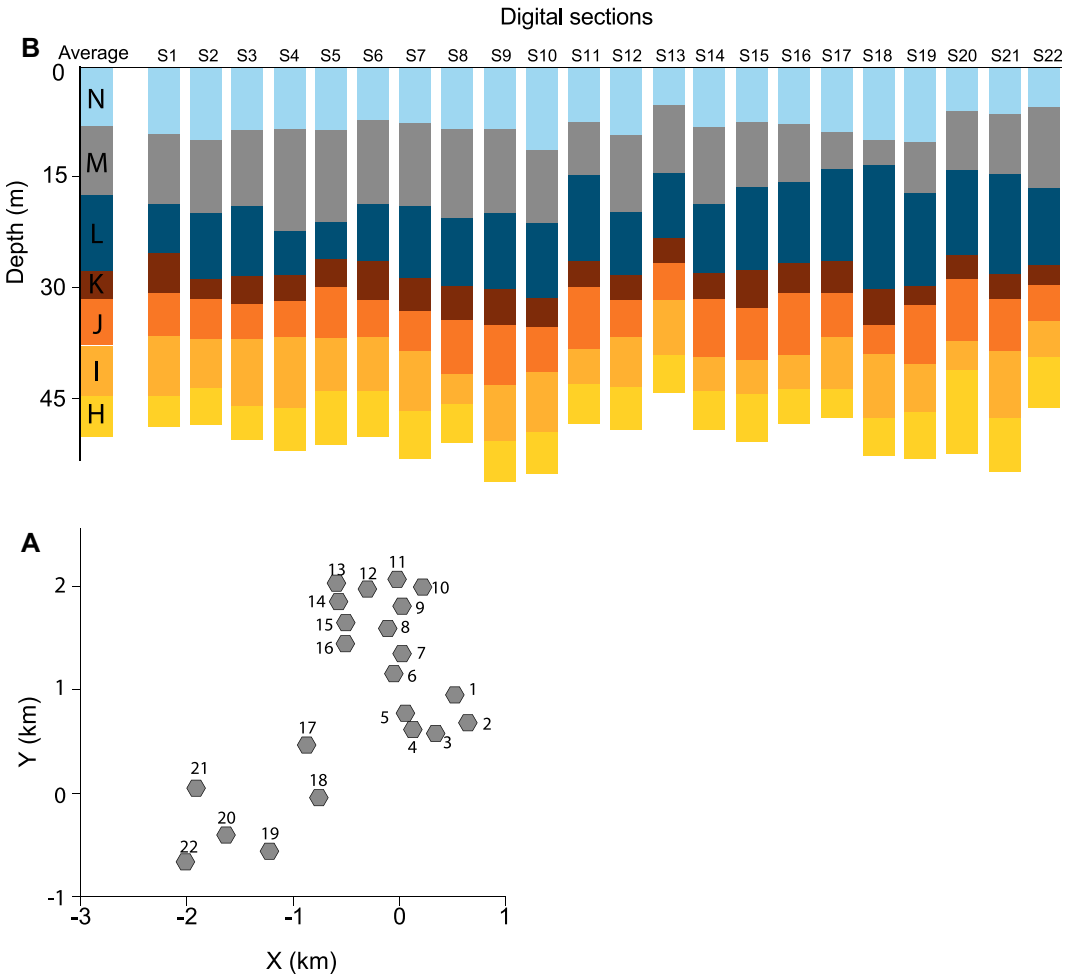

Figure 8. Variation of floodplain aggradation cycle thickness in the lateral extent in the McCullough Peaks area (Wyoming, USA). The lower panel displays the locations of 22 digital sections, while the upper panel shows the thickness variations of seven successive floodplain aggradation cycles, with the top floodplain aggradation cycle flattened. Note that the coordinates in the lower panel are converted from global Universal Transverse Mercator coordinates to local ones, with an applied offset of X offset = 673,000 m and Y offset = 49,242,600 m.

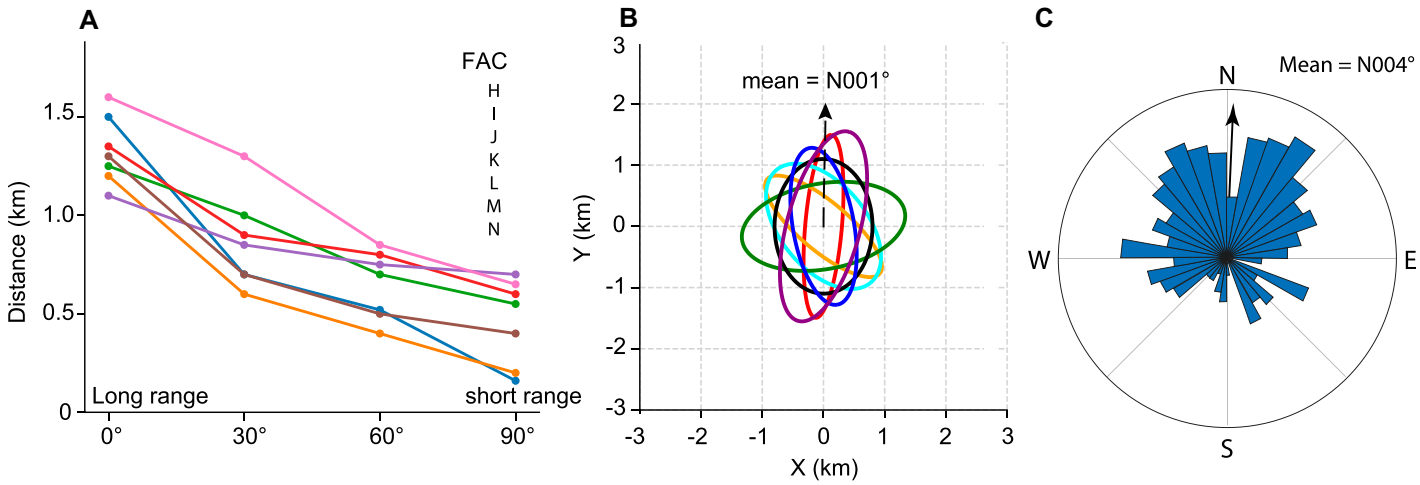

Figure 9. Variogram features of floodplain aggradation cycle thicknesses and flow directions measured in the field in the McCullough Peaks area (Wyoming, USA). (A) Variation of ranges with azimuth, assuming the long-range azimuth to be N 000° and thus the short-range azimuth to be N 090°. (B) Oriented variogram ellipses with long and short ranges as long and short axes. (C) Field-measured paleoflow directions in the dune-scale cross-stratifications (after Wang et al., 2022). FAC—floodplain aggradation cycle.

landscape, the properties of floodplain deposits may change significantly within 1–2 km in the direction perpendicular to paleoflow (Mohrig et al., 2000). However, the floodplain aggradation cycles studied here are the result of a long history of successive fluvial landscapes, each of which has its own local morphodynamic changes, including the movement of channel belts and local crevasse splays and avulsions. As a result, our field data relates to changing properties of complete floodplain aggradation cycles that have lasted ~20 k.y. (Abels et al., 2013, 2016; van der Meulen et al., 2020). Therefore, it can be inferred that the observed downstream consistency of floodplain aggradation cycles at 1–2 km scales reasonably suggests the consistency of fluvial landscapes over thousands of years, likely represented by the consistent paleoflow direction and channel belt orientation.

To conclude, the large lateral thickness variability of individual meter-scale floodplain aggradation cycles is mainly attributed to varying aggradation rates related to channel proximity, while the consistency of lateral thickness changes is related to the channel-belt orientation in paleoflow direction. Further refinement and quantification of the results should come from decompaction of the series through a dynamic backstripping exercise.

Vertical Thickness Variability of Floodplain Aggradation Cycles

Vertically, floodplain aggradation cycles with thicknesses below the average are often followed by cycles that are thicker than the average (Figs. 4 and 6). This tendency is further substantiated by a sequential reduction in the CV as a greater number of floodplain aggradation cycles are vertically stacked. Specifically, the CV decreases from 23% for single, individual cycles (i.e., those shown in Fig. 7) to 14% when considering the sum of two cycles, and it further diminishes to 10% for the cumulative sum of three cycles (Fig. 12). This suggests

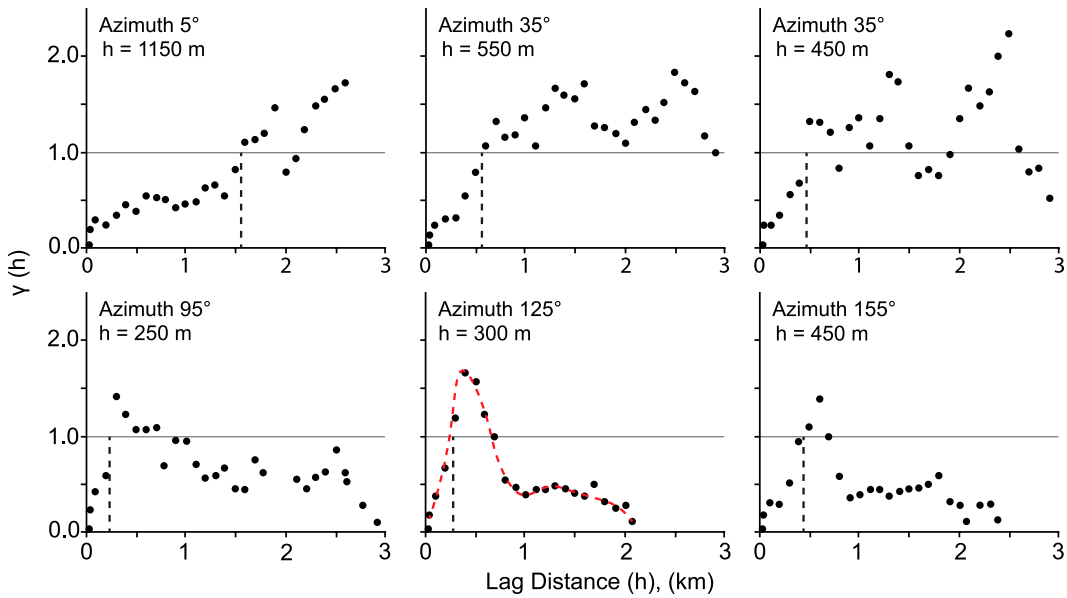

Figure 10. One-dimensional directional variograms for floodplain aggradation cycle H with different azimuths in the McCullough Peaks area (Wyoming, USA). Vertical dashed lines indicate the ranges along different azimuths. Red dashed line in the panel with azimuth 125° shows an example of a non-monotonic variogram that is different from traditional, monotonic ones (e.g., azimuth 5°). Information on how to read variograms is detailed in the Methodology section.

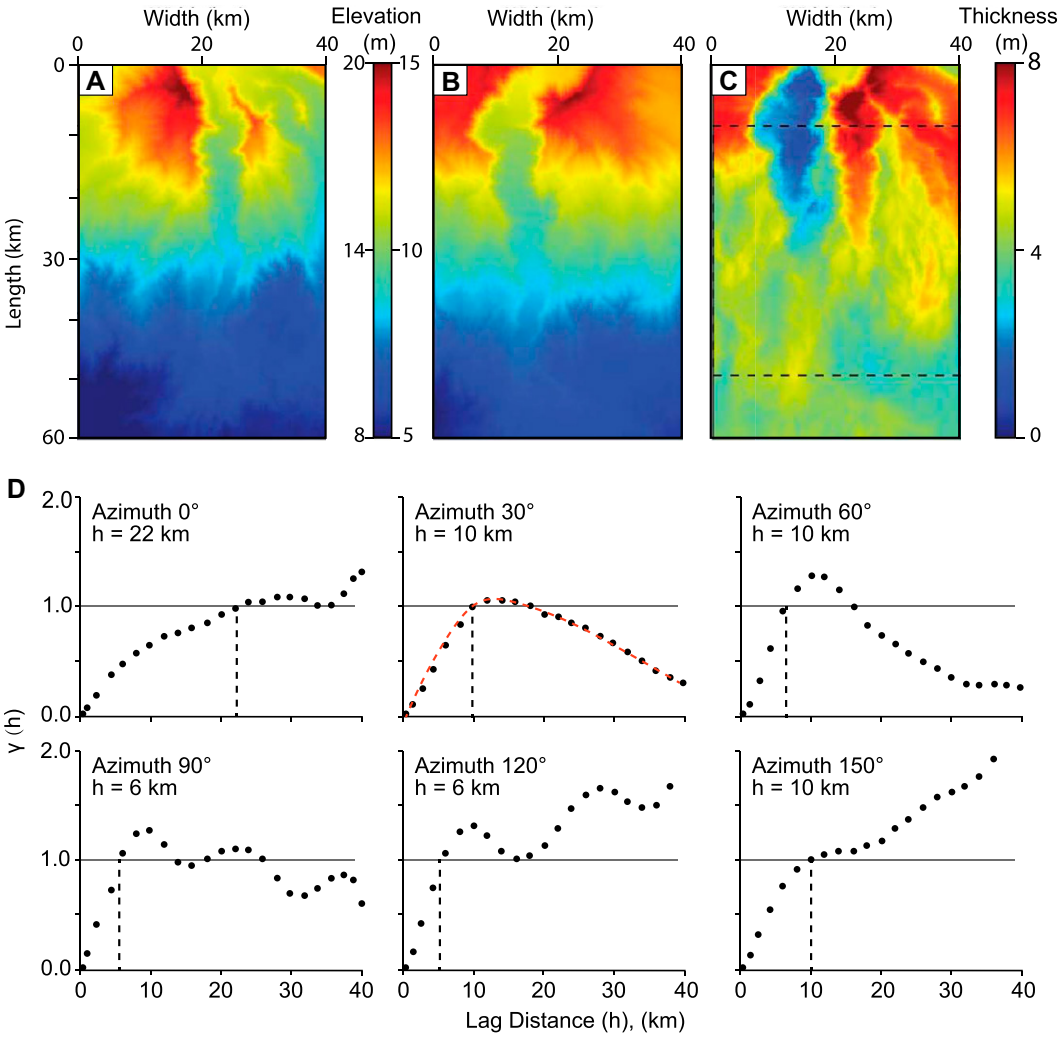

Figure 11. Geostatistical analysis using the Scenario A40 data produced by Wang et al. (2021). (A) The elevation map of the base of cycle 3. (B) The elevation map of the top of cycle 3. (C) The thickness map of cycle 3. (D) Directional variograms using the data constrained by dashed lines in panel C. Comparable, similar non-monotonic variograms, as those in Figure 10, are also observed.

that much of the vertical thickness variability is counterbalanced by variable deposition over two to three successive floodplain aggradation cycles. Full compensation of floodplain aggradation cycle thicknesses requires the stacking of at least six floodplain aggradation cycles in this analysis of our data (Fig. 12), which equates to an approximate thickness of 41 m (based on the average thickness of floodplain aggradation cycles from Fig. 6), corresponding to a time span of ~120 k.y. based on the long-term sedimentation rate (0.33 m/k.y.; Abels et al., 2013, 2016).

Our calculated T_c value of ~120 k.y. is longer than that estimated by Straub et al. (2020), which is 10–67 k.y. This discrepancy is expected because the method used by Straub et al. (2020) is based on the maximum channel-belt sandstone body thickness and long-term sedimentation rates in the Bighorn Basin, which is applicable when there is no external forcing. If these floodplain aggradation cycles are driven by allogenic forcing (as suggested by Abdul Aziz et al., 2008; Abels et al., 2013, 2016), T_c could extend by up to 2.5 times compared to an entirely autogenic scenario, as suggested by the modeling results of Wang et al. (2021). The underlying cause for this extension remains uncertain. It may be attributed to the pronounced lateral channel migration prompted by high-amplitude allogenic forcing, which consumes substantial, additional time alongside vertical channel aggradation (Barefoot et al., 2022; Wang et al., 2021).

Straub and Pyles (2012) proposed that units as small as individual channel beds are compensating for the topographic differences created by older beds, whereas units of channel stories and higher hierarchy (i.e., channel element and channel complex) are also compensating for one another during their stacking. We extend this concept to floodplain aggradation cycles, which also exhibit features of compensational stacking. Furthermore, this finding aligns with the conclusions reached by Trampush et al. (2017), who demonstrate that for data sets exceeding three times the thickness of a characteristic depositional element (such as a channel), compensation statistics can be reliably applied to constrain the maximum scale of autogenic sedimentation, even in the case of low-resolution data sets. In the present study, the stratigraphic resolution is delineated at the scale of floodplain aggradation cycles (averaging 6.8 m), a measurement considered low due to its proximity to the thickness of channel sandstone bodies (averaging 6.1 m for braided channel sandstone formations and 9.0 m for sinuous channel sandstone formations; Wang et al., 2022). Nevertheless, the stratigraphic sequence, ~300 m in length, significantly surpasses by three times the channel depth, thereby providing a reliably constrained compensational stacking index, denoted by $\kappa = 1$ (also see the extensive sensitivity tests in Trampush et al., 2017).

The average thickness of individual floodplain aggradation cycles varies between 3.7 m and 9.7 m for the seven cycles studied in detail (Fig. 7). There could be several reasons for this. First, if these floodplain aggradation

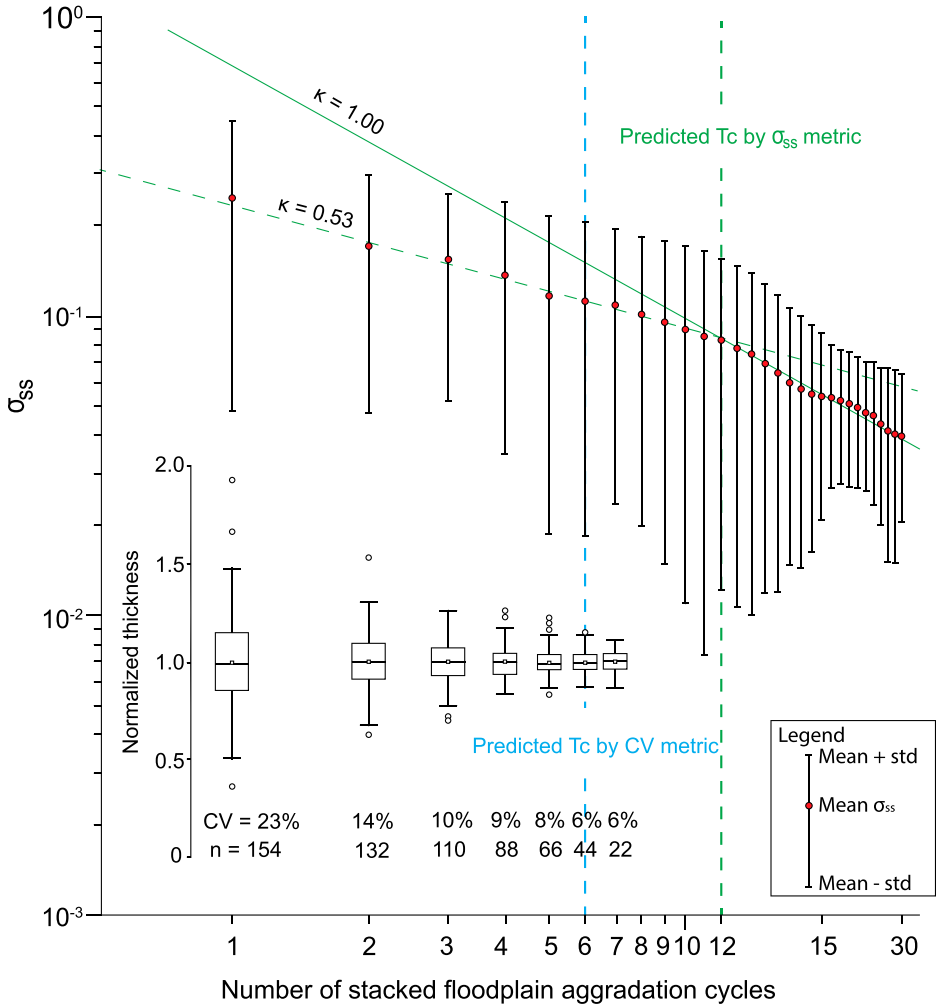

Figure 12. Two metrics for indicating the compensational time scale (T_c) based on floodplain aggradation cycle thicknesses in the McCullough Peaks area (Wyoming, USA). (1) The lower part shows the decay of the coefficient of variation (CV) with an increasing number of floodplain aggradation cycles in a stratigraphic assemblage. The predicted T_c corresponds to about six floodplain aggradation cycles since CV does not reduce any further and stabilizes at 6%. (2) The upper part shows the decay of σ_{ss} with an increasing number of floodplain aggradation cycles in the composite section. Red dots indicate the mean σ_{ss} at the corresponding number of floodplain aggradation cycles, error bars represent the geometric standard deviation (std) from the mean, green dashed and solid trend lines represent the best linear-fit of dots on the two sides of the knickpoint, and the vertical green dashed line indicates the predicted T_c (see Straub et al. [2009] and the Methodology section for a more detailed explanation of the principle) that corresponds to 12 floodplain aggradation cycles, over which the stratigraphic stacking transits from anti-compensational to compensational form.

cycles are driven by precession-scale climate change, as suggested in previous work (Abdul Aziz et al., 2008; Abels et al., 2013, 2016; van der Meulen et al., 2020), their deposition may represent different amounts of time since wavelengths of individual precession cycles dominantly range between 18.6 k.y. and 23 k.y. at present (Berger et al., 1992). Consequently, the impact of this discrepancy is anticipated to be ~24% (i.e., 23 k.y./18.6 k.y. − 1 = 0.24), a value relatively minor when contrasted with the disparity between the thickest and thinnest floodplain aggradation cycles (i.e., 9.7 m/3.7 m − 1 = 1.62) (Fig. 7). Alternatively, the thickness variations of the floodplain aggradation cycles may be governed by intricate interactions between precession, obliquity, and eccentricity, factors that collectively modulate insolation at Earth's atmospheric apex (Lourens et al., 2001). However, delineating these interactions remains an unattainable objective within the confines of this study.

Second, the study area of 10 km^2 may be insufficient to capture the basin-wide variability. River systems may have moved their courses over larger areas than the study area, resulting in an absence of coarse-grained material during the deposition of some floodplain aggradation cycles, thereby rendering them thinner. Conversely, a dominance of coarse-grained material during other floodplain aggradation cycles makes them thicker. To further investigate this hypothesis, again, a larger data set is needed to trace floodplain aggradation cycles over a larger distance. Westerhold et al. (2018) suggested that floodplain aggradation cycles are continuous in the current study area and the Gilmore Hill area, ~15 km away (Westerhold et al., 2018), a claim made without independent age constraints as correlations were made with the lower stratigraphic portions covering the Deer Creek Amphitheater section in the Deer Creek area in which no tie-points exist to correlate directly to the Gilmore Hill area. Enlarging the study area could be possible using the current methodology toward the east from the current location into the Whistle Creek area and ultimately the Gilmore Hill area. Such enlargement, coupled with the application of abovementioned dynamic backstripping to tackle the intricate nature of decompaction, constitutes our recommendations for future investigations in this field, as well as for analogous studies, contingent upon the availability of requisite resources.

Implications for Alluvial Stratigraphic Analysis

In alluvial stratigraphic analysis that aims to extract allogenic signals, it is essential to disentangle these signals from the lateral and vertical variability produced by autogenic processes. We recommend using composite stratigraphy averaged across multiple 1-D sections to mitigate the impact of lateral thickness variability. An approach for this is presented by Zhang et al. (2022) and similar techniques have been applied to paleoclimate records from ocean drilling data (e.g., Lisiecki and Raymo, 2005). The concomitant significant vertical thickness variability, which is partially interpreted to be influenced by autogenic processes, also poses a great challenge for allogenic signal extraction. It is imperative to approach the interpretation of meter-scale and kilo-year-scale variability in high-resolution paleoclimate records of 1-D alluvial stratigraphic records with circumspection (also see Foreman and Straub, 2017). The absence of continuity in sedimentation at scales below the compensational time scales and the equal spacing of sampling lead to highly unequal time series

in the resultant record. The combination of multiple 1-D records into composite stratigraphy may enhance the ability to generate high-resolution paleoenvironmental records from alluvial strata, thereby bolstering confidence in the findings.

CONCLUSIONS

Here, we utilize a 3-D photogrammetric model to examine the lateral and vertical thickness variability of floodplain aggradation cycles in the McCullough Peaks area of the lower Eocene Willwood Formation in the Bighorn Basin, Wyoming.

Laterally, the thicknesses of individual floodplain aggradation cycles may vary rapidly. This thickness variability is less pronounced along the paleoflow direction than across it. Such a pattern is postulated to be associated with the organization of fluvial landscapes over the depositional time, in congruence with paleoflow directions. The lateral thickness variability is attributed to the varied depositional rates away from the channel belts and the preferential filling of paleotopography by sedimentary processes during flooding events.

Vertically, there are significant thickness variations among successive cycles; thicker-than-average floodplain aggradation cycles tend to be followed by thinner ones as observed in both 1-D and 3-D mapping.

Strong compensational stacking is evident at the vertical scale of two to three floodplain aggradation cycles, while full compensational stacking occurs at the scale of at least six floodplain aggradation cycles. This scale exceeds previous estimates that were predicted on the absence of allogenic forcing. This finding underscores the complex interplay between allogenic forcing and autogenic processes, which serves to extend the compensational time scale.

Our findings emphasize the necessity of incorporating 3-D data to counterbalance the influence of substantial lateral thickness variation, while analyzing larger-scale stratigraphic patterns can help minimize the impact of vertical thickness variability. Therefore, when interpreting alluvial stratigraphy or using samples of alluvial stratigraphy to reconstruct paleoenvironments or paleoclimates, it is vital to systematically evaluate both the lateral and vertical dimensions, considering the inherent variability in thickness.

ACKNOWLEDGMENTS

This study was financially supported by Top Sectors GeoEnergie, Equinor, and Wintershall to H.A. Abels, J.E.A. Storms, A.W. Martinius, and T.F. Baars (FRESCO [Fluvial Reservoir Heterogeneity and Connectivity] Project, grant no. TKI2018-03-GE), a China Scholarship Council grant to Y. Wang (no. 201606440046), the Dutch Molengraaff fund to Y. Wang (Stichting Molengraaff Fonds), and the International Association of Sedimentologists/SEPM (Society for Sedimentary Geology) travel grants to Y. Wang that contributed to the 2019 field visit. The authors acknowledge the help from Chaowen Wang, Dirk-Jan Walstra, Hiranya Sahoo, and the Churchill family of Powell, Wyoming, for their help in the field, Jasper de Lanoy for the earlier photogrammetric models and model interpretations, and Suihong Song for discussion on variogram analysis. We thank the Ph.D. committee members of Y. Wang for their suggestions on the thesis chapter that was converted to the original manuscript, including Esther Stouthamer, Chris Fielding, Giovanni Bertotti, Gary Hampson, and Klaudia Kuiper. We also thank Sébastian Carretier, Jean-Philippe Avouac, Peter Burgess, Elizabeth Hajek, Associate Editor Zoltan Sylvester, Science Editor Brad Singer, and three anonymous reviewers for their thoughtful and helpful comments that allowed us to improve earlier versions of our manuscript.

REFERENCES CITED

Abdul Aziz, H., Hilgen, F.J., van Luijk, G.M., Sluijs, A., Kraus, M.J., Pares, J.M., and Gingerich, P.D., 2008, Astronomical climate control on paleosol stacking patterns in the upper Paleocene–lower Eocene Willwood Formation, Bighorn Basin, Wyoming: Geology, v. 36, p. 531–534, https://doi.org/10.1130/G24734A.1.

Abels, H.A., Clyde, W.C., Gingerich, P.D., Hilgen, F.J., Fricke, H.C., Bowen, G.J., and Lourens, L.J., 2012, Terrestrial carbon isotope excursions and biotic change during Palaeogene hyperthermals: Nature Geoscience, v. 5, p. 326–329, https://doi.org/10.1038/ngeo1427.

Abels, H.A., Kraus, M.J., and Gingerich, P.D., 2013, Precession-scale cyclicity in the fluvial lower Eocene Willwood Formation of the Bighorn Basin, Wyoming (USA): Sedimentology, v. 60, p. 1467–1483, https://doi.org/10.1111/sed.12039.

Abels, H.A., Lauretano, V., van Yperen, A.E., Hopman, T., Zachos, J.C., Lourens, L.J., Gingerich, P.D., and Bowen, G.J., 2016, Environmental impact and magnitude of paleosol carbonate carbon isotope excursions marking five early Eocene hyperthermals in the Bighorn Basin, Wyoming: Climate of the Past, v. 12, p. 1151–1163, https://doi.org/10.5194/cp-12-1151-2016.

Allen, J.R.L., 1978, Studies in fluviatile sedimentation: An exploratory quantitative model for the architecture of avulsion-controlled alluvial suites: Sedimentary Geology, v. 21, p. 129–147, https://doi.org/10.1016/0037-0738(78)90002-7.

Allen, P.A., 2008, From landscapes into geological history: Nature, v. 451, p. 274–276, https://doi.org/10.1038/nature06586.

Ashworth, P., Best, J., and Jones, M., 2004, Relationship between sediment supply and avulsion frequency in braided rivers: Geology, v. 32, p. 21–24, https://doi.org/10.1130/G19919.1.

Atchley, S.C., Nordt, L.C., and Dworkin, S.I., 2004, Eustatic control on alluvial sequence stratigraphy: A possible example from the Cretaceous-Tertiary transition of the Tornillo Basin, Big Bend National Park, West Texas, U.S.A.: Journal of Sedimentary Research, v. 74, p. 391–404, https://doi.org/10.1306/102203740391.

Atchley, S.C., Nordt, L.C., Dworkin, S.I., Cleveland, D.M., Mintz, J.S., and Harlow, R.H., 2013, Alluvial stacking pattern analysis and sequence stratigraphy: Concepts and case studies, *in* Driese, S.G., and Nordt, L.C., eds., New Frontiers in Paleopedology and Terrestrial Paleoclimatology: Paleosols and Soil Surface Analog Systems: SEPM (Society for Sedimentary Geology), v. 104, p. 109–129, https://doi.org/10.2110/sepmsp.104.13.

Barefoot, E.A., Nittrouer, J.A., Foreman, B.Z., Hajek, E.A., Dickens, G.R., Baisden, T., and Toms, L., 2022, Evidence for enhanced fluvial channel mobility and fine sediment export due to precipitation seasonality during the Paleocene-Eocene thermal maximum: Geology, v. 50, p. 116–120, https://doi.org/10.1130/G49149.1.

Berger, A., Loutre, M.F., and Laskar, J., 1992, Stability of the astronomical frequencies over the Earth's history for paleoclimate studies: Science, v. 255, p. 560–566, https://doi.org/10.1126/science.255.5044.560.

Birgenheier, L., Vanden Berg, M., Plink-Bjorklund, P., Gall, R., Rosencrans, E., Rosenberg, M.J., Toms, L.C., and Morris, J., 2020, Climate impact on fluvial-lake system evolution, Eocene Green River Formation, Uinta Basin, Utah, USA: Geological Society of America Bulletin, v. 132, p. 562–587, https://doi.org/10.1130/B31808.1.

Bridge, J.S., and Leeder, M.R., 1979, A simulation model of alluvial stratigraphy: Sedimentology, v. 26, p. 617–644, https://doi.org/10.1111/j.1365-3091.1979.tb00935.x.

Buckley, S.J., Ringdal, K., Naumann, N., Dolva, B., Kurz, T.H., Howell, J.A., and Dewez, T.J.B., 2019, LIME: Software for 3-D visualization, interpretation, and communication of virtual geoscience models: Geosphere, v. 15, p. 222–235, https://doi.org/10.1130/GES02002.1.

Burgess, P.M., 2016a, Identifying ideal stratigraphic cycles using a quantitative optimization method: Geology, v. 44, p. 443–446, https://doi.org/10.1130/G37827.1.

Burgess, P.M., 2016b, Identifying ordered strata: Evidence, methods, and meaning: Journal of Sedimentary Research, v. 86, p. 148–167, https://doi.org/10.2110/jsr.2016.10.

Célérier, B., 1988, How much does slip on a reactivated fault plane constrain the stress tensor?: Tectonics, v. 7, p. 1257–1278, https://doi.org/10.1029/TC007i006p01257.

Chadwick, A.J., Steele, S., Silvestre, J., and Lamb, M.P., 2022, Effect of sea-level change on river avulsions and stratigraphy for an experimental lowland delta: Journal of Geophysical Research: Earth Surface, v. 127, no. 7, https://doi.org/10.1029/2021JF006422.

Cleveland, D.M., Atchley, S.C., and Nordt, L.C., 2007, Continental sequence stratigraphy of the Upper Triassic (Norian Rhaetian) Chinle Strata, northern New Mexico, U.S.A.: Allocyclic and autocyclic origins of paleosol-bearing alluvial successions: Journal of Sedimentary Research, v. 77, p. 909–924, https://doi.org/10.2110/jsr.2007.082.

Clyde, W., Stamatakos, J., and Gingerich, P., 1994, Chronology of the Wasatchian land-mammal age (early Eocene): Magnetostratigraphic results from the McCullough Peaks section, northern Bighorn Basin, Wyoming: The Journal of Geology, v. 102, no. 4, https://doi.org/10.1086/629680.

Clyde, W.C., and Christensen, K.E., 2003, Testing the relationship between pedofacies and avulsion using Markov analysis: American Journal of Science, v. 303, p. 60–71, https://doi.org/10.2475/ajs.303.1.60.

Foreman, B.Z., 2014, Climate-driven generation of a fluvial sheet sand body at the Paleocene-Eocene boundary in north-west Wyoming (USA): Basin Research, v. 26, p. 225–241, https://doi.org/10.1111/bre.12027.

Foreman, B.Z., and Straub, K.M., 2017, Autogenic geomorphic processes determine the resolution and fidelity of terrestrial paleoclimate records: Science Advances, v. 3, https://doi.org/10.1126/sciadv.1700683.

Gingerich, P.D., 1969, Markov analysis of cyclic alluvial sediments: Journal of Sedimentary Petrology, v. 39, p. 330–332, https://doi.org/10.1306/74D71C4E-2B21-11D7-8648000102C1865D.

Gingerich, P.D., 2010, Mammalian faunal succession through the Paleocene-Eocene thermal maximum (PETM) in western North America: Vertebrata Pal Asiatica, v. 48, p. 308–327.

Gradstein, F.M., Ogg, J.G., and Hilgen, F.J., 2012, On The Geologic Time Scale: Newsletters on Stratigraphy, v. 45, p. 171–188, https://doi.org/10.1127/0078-0421/2012/0020.

Hajek, E.A., and Straub, K.M., 2017, Autogenic sedimentation in clastic stratigraphy: Annual Review of Earth and Planetary Sciences, v. 45, p. 681–709, https://doi.org/10.1146/annurev-earth-063016-015935.

Hajek, E.A., and Wolinsky, M.A., 2012, Simplified process modeling of river avulsion and alluvial architecture: Connecting models and field data: Sedimentary Geology, v. 257–260, p. 1–30, https://doi.org/10.1016/j.sedgeo.2011.09.005.

Jerolmack, D.J., and Mohrig, D., 2007, Conditions for branching in depositional rivers: Geology, v. 35, p. 463, https://doi.org/10.1130/G23308A.1.

Jones, L.S., and Schumm, S.A., 1999, Causes of avulsion: An overview, *in* Smith, N.D., and Rogers, J., eds., Fluvial Sedimentology VI: Oxford, UK, Blackwell Science, p. 169–178, https://doi.org/10.1002/9781444304213.ch13.

Karssenberg, D., and Bridge, J.S., 2008, A three-dimensional numerical model of sediment transport, erosion and deposition within a network of channel belts, floodplain and hill slope: Extrinsic and intrinsic controls on floodplain dynamics and alluvial architecture: Sedimentology, v. 55, p. 1717–1745, https://doi.org/10.1111/j.1365-3091.2008.00965.x.

Kraus, M.J., 1987, Integration of channel and floodplain suites, II. Vertical relations of alluvial paleosols: Journal of Sedimentary Petrology, v. 57, p. 602–612.

Kraus, M.J., 1999, Paleosols in clastic sedimentary rocks: Their geologic applications: Earth-Science Reviews, v. 47, p. 41–70, https://doi.org/10.1016/S0012-8252(99)00026-4.

Kraus, M.J., and Aslan, A., 1993, Eocene hydromorphic paleosols: Significance for interpreting ancient floodplain processes: SEPM Journal of Sedimentary Research, v. 63, no. 3, p. 453–463, https://doi.org/10.1306/D4267B22-2B26-11D7-8648000102C1865D.

Kraus, M.J., and Middleton, L., 1987, Contrasting architecture of two alluvial suites in different structural settings, *in* Ethridge, F.G., Fiores, R.M., and Harvey, M.D., eds., Recent Developments in Fluvial Sedimentology: Society of Economic Paleontologists and Mineralogists Special Publication 39, p. 253–262, https://doi.org/10.2110/pec.87.39.0253.

Lanci, L., Galeotti, S., Ratcliffe, K., Tohver, E., Wilson, A., and Flint, S., 2022, Astronomically forced cycles in middle Permian fluvial sediments from Karoo Basin (South Africa): Palaeogeography, Palaeoclimatology, Palaeoecology, v. 596, https://doi.org/10.1016/j.palaeo.2022.110973.

Lillegraven, J.A., and Ostresh, L.M., Jr., 1988, Evolution of Wyoming's early Cenozoic topography and drainage patterns: National Geographic Research, v. 4, p. 303–327.

Lisiecki, L.E., and Raymo, M.E., 2005, A Pliocene-Pleistocene stack of 57 globally distributed benthic $\delta^{18}O$ records: Paleoceanography and Paleoclimatology, v. 20, no. 1, https://doi.org/10.1029/2004PA001071.

Lourens, L., Wehausen, R., and Brumsack, H., 2001, Geological constraints on tidal dissipation and dynamical ellipticity of the Earth over the past three million years: Nature, v. 409, p. 1029–1033, https://doi.org/10.1038/35059062.

Mackey, S.D., and Bridge, J.S., 1995, Three-dimensional model of alluvial stratigraphy; theory and applications: Journal of Sedimentary Research, v. 65, p. 7–31, https://doi.org/10.1306/D42681D5-2B26-11D7-8648000102C1865D.

Mohrig, D., Heller, P.L., Paola, C., and Lyons, W.J., 2000, Interpreting avulsion process from ancient alluvial sequences: Guadalope-Matarranya system (northern Spain) and Wasatch Formation (western Colorado): Geological Society of America Bulletin, v. 112, p. 1787–1803, https://doi.org/10.1130/0016-7606(2000)112<1787:IAPFAA>2.0.CO;2.

Neasham, J.W., and Vondra, C.F., 1972, Stratigraphy and petrology of the lower Eocene Willwood Formation, Bighorn Basin, Wyoming: Geological Society of America Bulletin, v. 83, p. 2167–2180, https://doi.org/10.1130/0016-7606(1972)83[2167:SAPOTL]2.0.CO;2.

Noorbergen, L.J., Abels, H.A., Hilgen, F.J., Robson, B.E., de Jong, E., Dekkers, M.J., Krijgsman, W., Smit, J., Collinson, M.E., and Kuiper, K.F., 2018, Conceptual models for short-eccentricity-scale climate control on peat formation in a lower Palaeocene fluvial system, north-eastern Montana (USA): Sedimentology, v. 65, p. 775–808, https://doi.org/10.1111/sed.12405.

Noorbergen, L.J., Turtù, A., Kuiper, K.F., Kasse, C., Van Ginneken, S., Dekkers, M.J., Krijgsman, W., Abels, H.A., and Hilgen, F.J., 2020, Long-eccentricity regulated climate control on fluvial incision and aggradation in the Palaeocene of north-eastern Montana (USA): Sedimentology, v. 67, p. 2529–2560, https://doi.org/10.1111/sed.12710.

Olsen, H., 1994, Orbital forcing on continental depositional system—Lacustrine and fluvial cyclicity in the Devonian of East Greenland, *in* de Boer, P.L., and Smith, D.G., eds., Orbital Forcing and Cyclic Sequences: Oxford, UK, Blackwell Scientific Publications, p. 429–438, https://doi.org/10.1002/9781444304039.ch26.

Opluštil, S., Laurin, J., Hýlová, L., Jirásek, J., Schmitz, M., and Sivek, M., 2022, Coal-bearing fluvial cycles of the late Paleozoic tropics; astronomical control on sediment supply constrained by high-precision radioisotopic ages, Upper Silesian Basin: Earth-Science Reviews, v. 228, https://doi.org/10.1016/j.earscirev.2022.103998.

Owen, A., Ebinghaus, A., Hartley, A.J., Santos, M.G.M., and Weissmann, G.S., 2017, Multi-scale classification of fluvial architecture: An example from the Palaeocene-Eocene Bighorn Basin, Wyoming: Sedimentology, v. 64, p. 1572–1596, https://doi.org/10.1111/sed.12364.

Owen, A., Hartley, A.J., Ebinghaus, A., Weissmann, G.S., and Santos, M.G.M., 2019, Basin-scale predictive models of alluvial architecture: Constraints from the Palaeocene–Eocene, Bighorn Basin, Wyoming, USA: Sedimentology, v. 66, p. 736–763, https://doi.org/10.1111/sed.12515.

Pyrcz, M., 2020, GitHub repository, https://github.com/GeostatsGuy/ (accessed 1 May 2020).

Pyrcz, M., and Deutsch, C.V., 2003, The whole story on the hole effect: Geostatistical Association of Australasia Newsletter, v. 18.

Simpson, G., and Castelltort, S., 2012, Model shows that rivers transmit high-frequency climate cycles to the sedimentary record: Geology, v. 40, p. 1131–1134, https://doi.org/10.1130/G33451.1.

Slingerland, R., and Smith, N.D., 2004, River avulsions and their deposits: Annual Review of Earth and Planetary Sciences, v. 32, p. 257–285, https://doi.org/10.1146/annurev.earth.32.101802.120201.

Straub, K.M., and Pyles, D.R., 2012, Quantifying the hierarchical organization of compensation in submarine fans using surface statistics: Journal of Sedimentary Research, v. 82, p. 889–898, https://doi.org/10.2110/jsr.2012.73.

Straub, K.M., and Wang, Y., 2013, Influence of water and sediment supply on the long-term evolution of alluvial fans and deltas: Statistical characterization of basin-filling sedimentation patterns: Journal of Geophysical Research: Earth Surface, v. 118, p. 1602–1616, https://doi.org/10.1002/jgrf.20095.

Straub, K.M., Paola, C., Mohrig, D., Wolinsky, M.A., and George, T., 2009, Compensational stacking of channelized sedimentary deposits: Journal of Sedimentary Research, v. 79, p. 673–688, https://doi.org/10.2110/jsr.2009.070.

Straub, K.M., Duller, R.A., Foreman, B.Z., and Hajek, E.A., 2020, Buffered, incomplete, and shredded: The challenges of reading an imperfect stratigraphic record: Journal of Geophysical Research: Earth Surface, v. 125, no. 3, https://doi.org/10.1029/2019JF005079.

Törnqvist, T., Wallace, D., Storms, J., Wallinga, J., Van Dam, R., Blaauw, M., Derksen, M., Klerks, C., Meijneken, C., and Snijders, E., 2008, Mississippi Delta subsidence primarily caused by compaction of Holocene strata: Nature Geoscience, v. 1, p. 173–176, https://doi.org/10.1038/ngeo129.

Törnqvist, T.E., and Bridge, J.S., 2002, Spatial variation of overbank aggradation rate and its influence on avulsion frequency: Sedimentology, v. 49, p. 891–905, https://doi.org/10.1046/j.1365-3091.2002.00478.x.

Trampush, S.M., Hajek, E.A., Straub, K.M., and Chamberlin, E.P., 2017, Identifying autogenic sedimentation in fluvial-deltaic stratigraphy: Evaluating the effect of outcrop-quality data on the compensation statistic: Journal of Geophysical Research: Earth Surface, v. 122, no. 1, https://doi.org/10.1002/2016JF004067.

Vandenberghe, N., Hilgen, F.J., Speijer, R.P., Ogg, J.G., Gradstein, F.M., Hammer, O., Hollis, C.J., and Hooker, J.J., 2012, The Paleogene period, *in* Gradstein, F.M., Ogg, J.G., Schmitz, M.D., and Ogg, G.M., eds., The Geologic Time Scale: Boston, Elsevier, p. 855–921, https://doi.org/10.1016/B978-0-444-59425-9.00028-7.

van der Meulen, B., Gingerich, P.D., Lourens, L.J., Meijer, N., van Broekhuizen, S., van Ginneken, S., and Abels, H.A., 2020, Carbon isotope and mammal recovery from extreme greenhouse warming at the Paleocene–Eocene boundary in astronomically-calibrated fluvial strata, Bighorn Basin, Wyoming, USA: Earth and Planetary Science Letters, v. 534, https://doi.org/10.1016/j.epsl.2019.116044.

Wang, Y., Straub, K.M., and Hajek, E.A., 2011, Scale-dependent compensational stacking: An estimate of autogenic time scales in channelized sedimentary deposits: Geology, v. 39, p. 811–814, https://doi.org/10.1130/G32068.1.

Wang, Y., Storms, J.E.A., Martinius, A.W., Karssenberg, D., and Abels, H.A., 2021, Evaluating alluvial stratigraphic response to cyclic and non-cyclic upstream forcing through process-based alluvial architecture modelling: Basin Research, v. 33, p. 48–65, https://doi.org/10.1111/bre.12454.

Wang, Y., Baars, T.F., Sahoo, H., Storms, J.E.A., Martinius, A.W., Gingerich, P., and Abels, H.A., 2022, Sandstone body character and river planform styles of the lower Eocene Willwood Formation, Bighorn Basin, Wyoming, USA: Sedimentology, v. 69, no. 7, p. 2897–2924, https://doi.org/10.1111/sed.13027.

Westerhold, T., Röhl, U., Wilkens, R.H., Gingerich, P.D., Clyde, W.C., Wing, S.L., Bowen, G.J., and Kraus, M.J., 2018, Synchronizing early Eocene deep-sea and continental records: Cyclostratigraphic age models for the Bighorn Basin Coring Project drill cores: Climate of the Past, v. 14, p. 303–319, https://doi.org/10.5194/cp-14-303-2018.

Zachos, J.C., McCarren, H., Murphy, B., Röhl, U., and Westerhold, T., 2010, Tempo and scale of late Paleocene and early Eocene carbon isotope cycles: Implications for the origin of hyperthermals: Earth and Planetary Science Letters, v. 299, p. 242–249, https://doi.org/10.1016/j.epsl.2010.09.004.

Zhang, J., Jiang, Z., Liang, C., Baars, T.F., Wang, Y., and Abels, H.A., 2022, Astronomical forcing of meter-scale organic-rich mudstone–limestone cyclicity in the Eocene Dongying sag, China: Implications for shale reservoir exploration: AAPG Bulletin, v. 106, no. 8, p. 1557–1579, https://doi.org/10.1306/02072220103.

Zhang, Y., Person, M., Paola, C., Gable, C.W., Wen, X.-H., and Davis, J.M., 2005, Geostatistical analysis of an experimental stratigraphy: Geostatistical analysis of experimental stratigraphy: Water Resources Research, v. 41, no. 11, https://doi.org/10.1029/2004WR003756.

Science Editor: Brad Singer
Associate Editor: Zoltan Sylvester

Manuscript Received 28 April 2023
Revised Manuscript Received 21 August 2023
Manuscript Accepted 8 September 2023